Computational and Theoretical Chemistry 1022 (2013) 94–102

Contents lists available at ScienceDirect

Computational and Theoretical Chemistry

journal homepage: www.elsevier.com/locate/comptc

Structure and dynamics of the Th^{4+}-ion in aqueous solution – An *ab initio* QMCF-MD study

Lorenz R. Canaval *, Alexander K.H. Weiss, Bernd M. Rode

Theoretical Chemistry Division, Institute of General, Inorganic and Theoretical Chemistry, University of Innsbruck, Innrain 80-82, A-6020 Innsbruck, Austria

ARTICLE INFO

Article history:
Received 16 July 2013
Received in revised form 20 August 2013
Accepted 23 August 2013
Available online 2 September 2013

Keywords:
Thorium
QMCF-MD
Structure of liquids
Ab initio calculations
Hydration structure
Intrashell dynamics

ABSTRACT

An *ab initio* quantum mechanical charge-field molecular dynamics simulation of the tetravalent thorium ion in aqueous environment is presented. Including the first and second hydration shell in the quantum mechanical treatment to enhance accuracy, this study yields very good results for a wide range of characteristics, as compared to experimental data. 20 ps of simulation time were used to investigate structural and dynamical properties of the hydrate by numerous methods, including radial and angular distribution functions, three-body distribution functions, ligand exchange analysis and vibrational spectra. The hydrate proved stable during the simulation and did not show hydrolysis. The first solvation shell was found to be a very flexible one, with a number of intrashell ligand rearrangements occurring along the simulation. The data of the simulation also indicated the existence of a third hydration layer. Vibrational analysis yielded an average ion–oxygen frequency of 420 cm^{-1}, which is in excellent agreement with experimental data.

1. Introduction

Due to numerous incidents in nuclear power-plants and the resulting environmental concern, the properties of radioactive species such as U^{4+}, Th^{4+} received increasing interest. Thorium serves as nuclear fuel which was demonstrated by several prototypes of nuclear power reactors using thorium compounds since the mid 1950s [1]. Recently, this application received attention due to efforts to develop high-temperature pebble-bed reactors [2]. It has been reported that one of the major advantages of this type of reactor is that "*it is not physically possible to cause a meltdown*" [3]. Another benefit of thorium compared to uranium is that it is three times more abundant in nature [1]. Moreover it is possible to use ^{232}Th for breeding the fissile isotope ^{233}U via neutron irradiation followed by beta decay of ^{233}Pa.

As thorium occurs in various lanthanoid-containing ores [4,5], it also raised environmental concerns as by-product of rare earth element mining and processing. Neodymium, a key ingredient in the strong neodymium–iron–boron (NdFeB) magnets widely employed as components in electric generators for wind turbines, electric motors and hard disks, is a particularly prominent example. Since wind power is widely considered as clean energy source, the use of NdFeB magnets and the resulting accumulation of environmental toxins such as thorium has been termed "*Wind energy's dirty little secret*" on different occasions [6–8].

Over the last decades numerous groups have published studies on extraction, preconcentration and separation of thorium(IV) in aqueous solution. An overview publication on preconcentration techniques for uranium(VI) and thorium(IV) prior to analytical determination by Rao et al. from 2005 shows a wide range of on-line and off-line methods investigated, including liquid–liquid extraction, liquid membranes, ion exchange, extraction chromatography, flotation, solid phase extraction and adsorptive accumulation [9]. Since 2005, many investigations on sorption of thorium(IV) on different pure and modified minerals and rocks (muscovite [10], goethite [11], attapulgite [12,13], clinoptilolite [14], Na-bentonite [15], poly (methacrylic acid)-grafted chitosan/bentonite composite [16], modified mesoporous silica [17], heulandite-analog [18], magnetite and ferrihydrite [19], perlite [20], diatomite [21], modified Amazon clays [22], bentonite [23], Na-rectorite [24], γ-alumina [25], TiO_2 nanoparticles [26], nanoparticles of anatase [27], silica [28], zeolitic volcanic tuff [29], gibbsite [30]), diverse other matrices [31–42], and even olive cake [43] and olive stones [44] were published. Moreover, there were efforts to construct selective membrane electrodes [45,46] and a coated wire thorium ion selective electrode [47,48] for the determination of thorium(IV) ions in solutions.

In spite of this huge amount of advanced studies, only few information is available on the very basic solvation properties of Th^{4+} in aqueous environment. Nonetheless, the great interest in this topic is emphasized by a very recent combined experimental and theoretical study on the hydration structure of thorium(IV) halides [49].

* Corresponding author. Tel.: +43 512 507 57150; fax: +43 512 507 57199.
E-mail address: lorenz.canaval@uibk.ac.at (L.R. Canaval).

2210-271X/$ - see front matter © 2013 Elsevier B.V. All rights reserved.
http://dx.doi.org/10.1016/j.comptc.2013.08.020

The data presented within this work based on the QMCF-MD (quantum mechanical charge field molecular dynamics) framework [50,51], which has proven its quality in many theoretical studies on ions all over the periodic table in the past, is of importance for further investigations on processing and recycling thorium containing nuclear waste. For this reason the data presented in this study is not only focused on structural properties, but also the dynamics of hydrated thorium(IV), which is one of few tetravalent species stable in aqueous solution.

2. Methods

2.1. Simulation method

The employed QMCF-MD ansatz [50] is based on the hybrid quantum mechanical–molecular mechanical (QM–MM) approach [52–54], where the main concept is to divide the system into two subregions. The first one contains the chemically interesting species, for example a solvated ion or molecule with its first hydration shell. Being the most relevant part of the simulation, the evaluation of energies and forces in this region is done by quantum mechanical means. In contrast, the remaining part of the system is treated classically. Thus, the goal is to achieve an affordable computational complexity for the system, but still high accuracy for the chemically important species.

The QMCF-MD methodology further improves the QM–MM approach by increasing the quantum mechanical treated subregion, and separating it into two zones: the core zone and the layer zone. Since the interatomic distances between QM particles in the core zone and MM atoms are usually greater than the non-Coulombic cutoff values, these contributions can be neglected. On the other hand, QM particles in the layer zone close to the MM region have small interatomic distances, and, therefore, non-Coulombic interactions have to be evaluated (Eq. (2)). Consequently, if the solute species (e.g. an ion and its first hydration shell) is kept in the inner QM region, while solute molecules only are present in the outer QM region (e.g. another solvation shell), a very convenient advantage of the QMCF-MD approach becomes evident: no complicated solute–solvent potential functions have to be constructed, as the interactions are treated via quantum mechanics, including many-body effects, charge transfer and polarization effects (Eq. (1)).

Secondly, the QMCF-MD approach makes use of an electrostatic embedding technique. A perturbation of the Hamiltonian of the quantum mechanical region is achieved by taking into account the atomic point charges of all atoms in the classical subregion. This concept prevents the QM region to expand its electron density into the virtual vacuum space surrounding it. The forces can thus be characterized as following:

$$F_j^{core} = F_j^{QM} \tag{1}$$

$$F_j^{layer} = F_j^{QM} + \sum_{i=1}^{M} \frac{q_i^{MM} q_j^{QM}}{r_{ij}^2} \left[1 + 2 \frac{\epsilon + 1}{2\epsilon - 1} \left(\frac{r_{ij}}{r_c} \right)^3 \right] + \sum_{i=1}^{M} F_{ij}^{non-coulomb} \tag{2}$$

$$F_j^{MM} = \sum_{i=1; i \neq j}^{M} F_{ij}^{MM} + \sum_{i=1}^{N_1+N_2} \frac{q_i^{MM} q_j^{QM}}{r_{ij}^2} \left[1 + 2 \frac{\epsilon + 1}{2\epsilon - 1} \left(\frac{r_{ij}}{r_c} \right)^3 \right] + \sum_{i=1}^{M} F_{ij}^{non-coulomb} \tag{3}$$

where F_j^{core} corresponds to the quantum mechanical force acting on a particle J in the core region, F_j^{layer} denotes the force acting on a particle J located in the layer region of the quantum mechanical zone, F_j^{MM} represents the force acting on a particle J in the classically treated region.

The application of solvent–solvent potentials within the MM region, and between the MM particles and the QM particles in the layer zone is standard practice. In this work, the flexible BJH-CF2 [55,56] water model including explicit hydrogen movements has been applied. For the evaluation of the QM–MM Coulombic forces, partial charges derived from Mulliken population analysis [57,58] are repetitively computed in every step of the simulation.

Particles can be exchanged between the QM and the MM subregions, which could lead to discontinuities. To avoid the latter, a small layer (typically 0.2 Å) is introduced at the QM/MM interface region. The forces of particles within this layer are evaluated on the basis of two different formula: first by the regular definition for the layer region $\left(F_j^{layer}\right)$, and second by assuming that the particle is part of the MM region $\left(F_j^{MM}\right)$ already. A smoothing function is employed to balance the two contributions, which results in a force F_j^{smooth}:

$$F_j^{smooth} = S(r)\left(F_j^{layer} - F_j^{MM}\right) + F_j^{MM} \tag{4}$$

where the smoothing factor $S(r)$ is defined by a continuous function gradually increasing from 0 to 1:

$$S(r) = \begin{cases} 1 & \forall r \leqslant r_1 \\ \frac{\left(r_0^2 - r^2\right)^2 \left(r_0^2 + 2r^2 - 3r_1^2\right)}{\left(r_0^2 - r_1^2\right)^3} & \forall r_{1<r\leqslant r_0} \\ 0 & \forall r > r_0 \end{cases} \tag{5}$$

where r describes the distance between the center of the QM region and the center of mass of a molecule, r_0 is the total radius of the QM region and r_1 is the inner border of the smoothing zone.

The increased accuracy of QMCF-MD simulations result in a significantly higher computational effort. Nonetheless, the methodology has been successfully applied to many systems, ranging from various cations [59] and anions [59] from all over the periodic table to small organic molecules in aqueous solution [60,61,51], proving its high quality.

2.2. Structural evaluation

Simple spherical radial distribution functions (RDFs) were evaluated, where the deviations from purely statistical distributions are plotted as a function of the distance between two particles, respectively [62]. In addition, angular distribution functions (ADFs) for the O–Ion–O angle were evaluated to investigate the geometrical arrangement of the first shell coordinating water molecules.

Solvation structure and solvent reorganizations of the ions were investigated via local density corrected three-body distribution functions $f_{O-X-O}^{(3)}(s,r,s)$ [63] (Eq. (6)) for each hydration shell observed. This analysis method is introduced to enable a comparison of different sub-regions within a hydrate, as well as different systems. The correction term includes ρ_{Shell} (Eq. (7)), which is a measure of the average density of a respective shell. Wherever the perturbations of the solvent due to the presence of a solute are of interest, pair distribution functions are not sufficient, because they are not significantly responsive to reorganizations, as the majority of contributions result from the solvent particles residing in bulk, where no reorganizations take place [63]. Three-body distributions [51] represent deviations in terms of the number of triangles, similar to pair distribution functions, where a deviation from the particle density of an ideal system is computed. Assuming the solute at the center and both solvent particles within the distance of $s \pm \Delta s/2$, the probability of finding a solvent–solvent distance of r defines the three-body correlation [63]

$$f_{O-X-O}^{(3)}(s,r,s) = \frac{\langle N^{(3)}(s,r,s) \rangle}{8\pi^2 N_X \rho_{Shell}^2 r s^2 \Delta s^2 \Delta r} \tag{6}$$

with N_X being the number of species X in the system, s being the average of the lower and upper border of the shell and Δs being the half of the shell width. The average density ρ_{Shell} is defined as

$$\rho_{\text{Shell}} = \sqrt{N_{\text{Shell}}(N_{\text{Shell}} - 1)/V_{\text{Shell}}^2} \quad (7)$$

where N_{Shell} corresponds to the average shell population of each configuration in a simulation and V_{Shell} denotes to the shell volume.

2.3. Evaluation of dynamics

To investigate ligand exchange dynamics within the hydration shells of the solutes, mean residence times (MRTs) of the water molecules of each shell were computed using the direct method [64]. The t^* value was set to 0.0 and 0.5 ps to study the exchange processes. Comparing the number of all transitions ($t^* = 0.0$) to the number of successful exchange events lasting at least 0.5 ps, the sustainability of the exchange processes is calculated. The average number of attempts needed to perform a successful exchange can be derived by taking the inverse of this value.

In order to investigate vibrational frequencies from a simulation trajectory, velocity autocorrelation functions (VACFs) must be evaluated [65,66] using normal coordinate analysis. The normalized VACF $C(t)$ is given by Eq. (8).

$$C(t) = \frac{\sum_i^{N_t}\sum_j^{N} v_j(t_i)\, v_j(t_i + t)}{\sum_i^{N_t}\sum_j^{N} v_j(t_i)\, v_j(t_i)} \quad (8)$$

N is the number of particles, N_t corresponds to the number of time origins t_i and v_j denotes a velocity component of particle j. To obtain the associated power spectrum, a Fourier transformation of the VACFs has to be performed.

Frequencies obtained from gas-phase HF calculations can suffer from a systematic error due to the neglect of electron correlation and the *in vacuo* environment and should, therefore, be scaled by a factor of 0.89 [67,68]. However, no such correction for the values obtained from the simulation presented here is necessary because of the small contribution of electron correlation, the electrostatic embedding technique applied to the quantum mechanical region, avoiding vacuum artifacts in the QM treatment and the explicit inclusion of anharmonicity in molecular dynamics simulations.

2.4. Simulation protocol

The simulation of one Th^{4+} cation in a 1000 water box was carried out at 298.15 K. The Berendsen weak coupling thermostat [69] was used with a relaxation time of 0.1 ps. The simulation box was defined cubic with the density of pure water at room temperature (0.997 g/cm^3), resulting in a side length of 31.2 Å. The radii of the quantum mechanical core zone and the layer zone were set to 3.1 Å and 5.7 Å, respectively. To overcome discontinuities of forces, a smoothing zone of 0.2 Å was applied. An Adams–Bashforth predictor–corrector algorithm was used to integrate the equations of motion with a time step of 0.2 fs. To correct the cutoff of the long-range electrostatic interactions above 15.0 Å, the reaction field method [70] was used ($\epsilon = 78.36$). In order to ensure bulk-like environment, periodic boundary conditions and the minimum image convention were applied. The simulation box of the previously investigated Ce^{4+} cation [71] was used as starting geometry and was equilibrated at 298.15 K for 3 ps with the Th^{4+} ion. After this, 20 ps of sampling time followed. In total 115000 MD steps have been carried out on a 12 CPU core system with an average loop time of about 230 s. All QM calculations within the simulation were executed with the TURBOMOLE 6.3 package [72–74].

Dunning double-ζ basis sets [75] with polarizing functions were chosen for hydrogen and oxygen, because they had already been successfully employed in previous simulation studies of aqueous solutions. For thorium, basis sets found in the EMSL database [76,77] (CRENBL ECP [78], Stuttgart RLC ECP [79], Stuttgart RSC 1997 ECP [79]) were tested by performing gas-phase geometry optimizations of $[Th(H_2O)_n]^{4+}$ clusters (n = 1, 2, 4, 6, 9) on four different levels of theory (B3LYP, Hartree–Fock, Møller–Plesset/2 and CCSD). These calculations were carried out with the GAUSSIAN 03 [80] software package. Although B3LYP showed slightly better values for the mean ion–water distance (2.54 Å for all three basis sets, irrespective of employing a small-core ECP or a large-core ECP) compared to Hartree–Fock (2.56 Å for all three basis sets) this functional was not choosen as it is known to "*overrate the rigidity of the water structure resulting in slower exchange rates*" [81]. It has been reported that also "*PBE and BLYP functionals under predict the density and over structure the liquid*" [82]. In addition it has been shown that these two functionals predict a far too high melting point for water (>400 K) on the one hand and "*suggested that the liquid phase is supercooled below the melting temperature*" [83] on the other hand. Correlated methods showed a slight decrease of total energy (0.28% and 0.25% for the $[Th(H_2O)_9]^{4+}$ cluster calculated with MP2 and CCSD, respectively, compared to HF) and a slight change of the ion–oxygen bond length (contraction to 2.53 Å and elongation to 2.58 Å for the $[Th(H_2O)_9]^{4+}$ cluster calculated with MP2 and CCSD, respectively, compared to HF). In summary, DFT seems not be the right choice when aiming to study dynamics of solvated species in aqueous environment whereas correlated methods are still not affordable in terms of computational effort.

To investigate the influence of the different approaches accounting for relativistic effects the cluster optimizations have not only been performed with basis sets employing small-core and large-core ECPs, but also for segmented all-electron relativistically contracted (SARC) basis sets employing the Douglas–Kroll–Hess (DKH) approximation and the zeroth order regular approximation (ZORA) [84]. It was found that these basis sets show even larger thorium–water distances for the 9-fold coordinated ion (2.58 Å for both HF and B3LYP). An approach treating the system fully relativistically would probably be a remedey for this dilemma, but this is computationally infeasible.

Finally, the Hartree–Fock level of theory and the CRENBL ECP basis set with a relativistically corrected ECP accounting for 78 inner electrons and treating the 12 outermost electrons explicitly were identified as adequate compromise between accuracy and computational effort.

3. Results and discussion

3.1. Structural aspects

3.1.1. Radial ordering

Fig. 1 shows the Th–O and Th–H RDFs and their integration curves. Th^{4+} forms two well-defined hydration spheres, the first one ranging from 2.25 to 3.13 Å, and the second one from 3.30 to 5.70 Å. The RDFs also show the formation of a weak third hydration shell between 5.70 and 7.90 Å, indicating the ion's strongly polarizing nature. The maxima for the Th–O and Th–H radial distribution functions are located at 2.54 and 3.12 Å for the first hydration shell, and at 4.65 and 5.37 Å for the second one.

The mean first-shell Th–O distance of 2.54 Å is in fair agreement with experimental data: EXAFS (Extended X-ray Absorption Fine Structure) measurements by Moll et al. [85] and Sandström et al. [86] indicated a Th–O distance of 2.45–2.49 Å, the work of Hennig et al. [87] a value of 2.44 Å, Rothe et al. [88] found a value of 2.45–2.46 Å, both groups using EXAFS technique too. LAXS (large angle X-ray scattering) investigations of thorium(IV) in aqueous perchlorate solutions by Johansson et al. [89] revealed a value of 2.48 Å. In an HEXS (high-energy X-ray scattering) study on $[Th(H_2O)_{10}]Br_4$ Th–O distances of 2.492(3) and 2.520(5) Å were reported for the prismatic and the capping water molecules, respectively [90]. Moreover, the results presented in this work are in agreement with

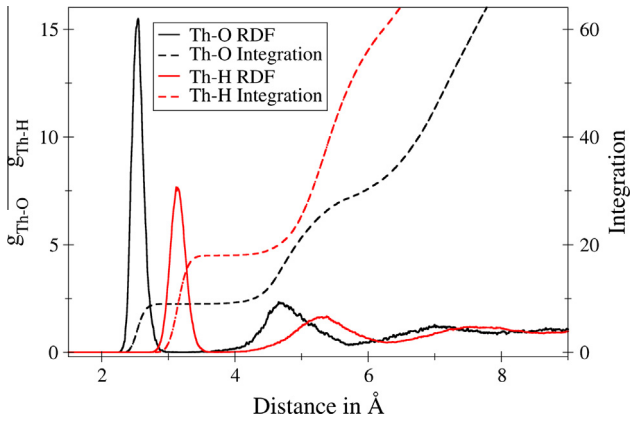

Fig. 1. Th–O (black) and Th–H (red) radial distribution functions (solid lines), including their integration information (dashed lines). (For interpretation of the references to color in this figure legend, the reader is referred to the web version of this article.)

recent theoretical investigations of tetravalent thorium in aqueous environment, using the concept of the hydrated ion [91] and classical MD-simulations [92]. The moderately elongated Th–O bond compared to experiments may have the following reasons: First, the Hartree–Fock method does not account for electron correlation contributions, which could narrow the bond as the gas-phase geometry optimizations of aqua-thorium(IV) clusters showed. Another reason could be that relativistic corrections are not sufficient in the effective core potential being employed.

The second maximum for the Th–O distribution at 4.65 Å is in good agreement with LAXS studies on thorium(IV) by Johansson et al. [89,91], which suggest a value of 4.6 Å.

3.1.2. Angular ordering

The ADF calculated from the simulation is shown in Fig. 2, where also a comparison to the ADF peaks expected for a perfect monocapped square antiprism and a perfect tricapped trigonal prism is given. Two peaks around 69.5° and 136.5° were found, connected through a valley ranging from 90° to 120°. The existence of this non-zero valley indicates rearrangements of first shell ligands between the two main angles. Furthermore, the peaks observed are not exclusively assignable to one of the idealized structures, but appear to be a mixture of both. In fact, a monocapped square antiprism and a tricapped trigonal prism are very similar: the root-mean-square deviation (RMSD) in terms of atom positions between the two perfect coordination polyhedra was calculated to be 0.374 Å. Considering the half-width of the peak of the first hydration shell in the Th–O RDF, a value of about 0.7 Å is obtained, which is nearly twice this RMSD value.

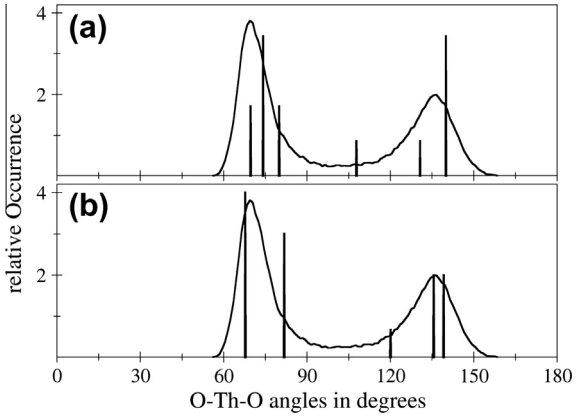

Fig. 2. O–Th–O angular distribution function for the first hydration shell of thorium(IV) in comparison to (a) a perfect monocapped square antiprism, (b) a perfect tricapped trigonal prism (bars).

3.1.3. Coordination number distribution

The CNDs of the first, second, and third shells are depicted in Fig. 3. The first hydration shell shows a stable 9-fold coordination. No water exchange reactions with the second shell took place during the simulation time of 20 ps. Experimental data show a great variation of the coordination number in the first shell: 8 ± 0.5 (LAXS) [89], 9.1 (NMR) [93], 9.8 (EXAFS) [87], 10 ± 1 (EXAFS) [85] and 11.6–12.7 (EXAFS) [88]. In general, the variation of coordination numbers reported in EXAFS studies is large. In addition, Soderholm et al. have demonstrated that the counter-ions play a crucial role on the structure of the first hydration shell [90] and stated that "*it is not possible to rule out an equilibrium in solution of 9-, 10-, and/or 11-coordinate thorium*" [90]. Only small differences in energy were reported between 9-, 10-, and 12-fold coordinated species for different theoretical approaches employing molecular dynamics simulations or quantum mechanical calculations [94–96,91]. Other studies indicate that a first hydration shell containing 9 water molecules is the most stable [91].

The second hydration shell shows an average coordination number of 19.8 water molecules. Again, this value agrees very well with experimental data: According to EXAFS studies by Johansson et al., in dilute perchlorate solution a distinct second hydration shell can be observed, which contains about 20 water molecules [89]. In addition, "*Gusev estimated the hydration number of the Th(IV) ion from the dependence of conductance on concentration in $NaClO_4$–$HClO_4$ solutions, and found the second hydration number to be 20*", too [91,97].

3.1.4. Local density corrected three-body distribution functions

To analyze the solvation structure and solvent reorganizations of thorium(IV) in more detail, local density corrected three-body distribution functions $f^{(3)}_{O-X-O}(s,r,s)$ [63] were evaluated for each hydration shell. According to the Th–O radial distribution function (see Fig. 1), the lower and upper boundaries defining the subregions utilized to evaluate the three-body distribution were set to the following values: 1st shell: 0.0–3.0 Å; 2nd shell: 3.2–5.7 Å; 3rd shell: 5.7–7.9 Å; 4th shell: 7.9–10.0 Å. The resolution was set to a value of 0.025 Å. To investigate the perturbation of the solvent structure due to the solute ion, the three-body distributions were compared to the O–O radial distribution function of pure water. Two broad and connected peaks at 2.90 and 4.70 Å are observed in the diagram for the first hydration shell (see Fig. 4). Even though no water exchanges took place between the first and second

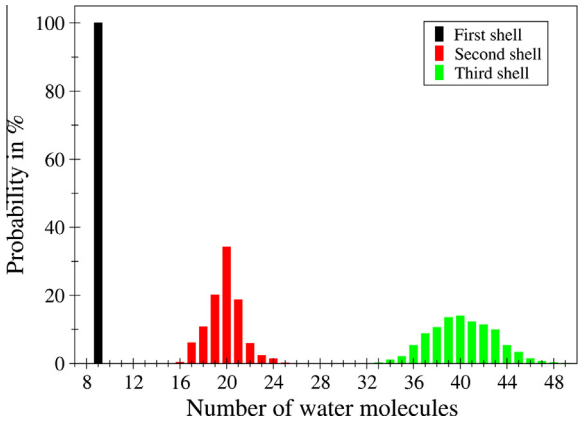

Fig. 3. Coordination number distribution for the first, second and third hydration shell of the Th^{4+} ion.

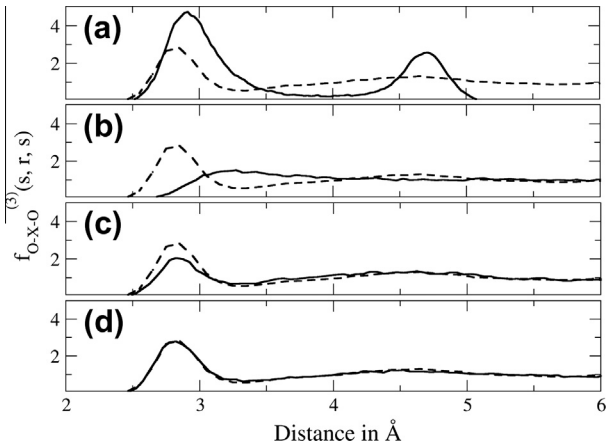

Fig. 4. Local density corrected three-body distribution functions for O–Th–O in (a) the first, (b) the second, (c) the third and (d) beyond the third hydration shell (solid lines) compared to the O–O RDF of pure solvent (dashed line).

hydration shell during the simulation, the connection of the two peaks in the three-body distribution function indicates rearrangements in the first solvation layer, which were further investigated via dihedral analysis (see next section). Thus, the first hydration shell surrounding the Th^{4+} ion can be considered a very flexible one. Due to the strongly polarizing nature of the ion investigated, the second and even the third solvation layer clearly differ from bulk water. In contrast, no additional fourth hydration layer can be observed beyond the distance of 7.9 Å, since in this volume the three-body correlation $f^{(3)}_{O-X-O}(s, r, s)$ coincides with the pair distribution of the bulk solvent (see Fig. 4d).

Recent studies on the highly charged ions Al^{3+} [98], Ce^{4+} [71], Zr^{4+} [99], Hf^{4+} [100] and U^{4+} [101] have revealed an ordering of water molecules up to the third hydration layer, too.

3.1.5. Dihedral angles

To understand the structure of the first hydration shell around the thorium(IV) ion in more detail, an analysis of dihedral angles was performed (see Fig. 5). Each line in the plot represents the evolution of a selected improper dihedral angle defined via the O–Th–O–O sequence along the simulation trajectory. A value of zero degrees in the plot represents planarity of three oxygens and the thorium ion. The structure is supposed to be tricapped trigonal prismatic when *one* of these groups is planar with the corresponding dihedral value oscillating around a value of 0°, as indicated in Fig. 5b (black oxygens capping), d (red oxygens capping) and f (blue oxygens capping). The transition between those structures was identified to proceed via a monocapped antiprismatic intermediate, *all three* of the O–Th–O–O dihedrals indicating planarity at the same time as can be seen in the respective snapshots Fig. 5c and e. Despite the inertness of the first shell showing no ligand exchange between the first and second hydration shell, a number of rearrangements in the first hydration layer were observed, thus suggesting it to be very flexible on the timescale of picoseconds.

3.1.6. Oxygen–oxygen distances

To further investigate the intrashell dynamics of the first hydration layer the evolution of all oxygen–oxygen-distances along the simulation trajectory was analyzed (see Fig. 6). To improve the visualization, running averages of 2 ps have been plotted. The dashed line in Fig. 6 corresponds to the minimum of the local density corrected three body distribution function for the first shell as shown in Fig. 4a, and it can be concluded that each crossing of this border is connected with an internal rearrangement of the structure of the first hydration layer. The plot clearly shows many of these reordering events to occur, in full agreement with the conclusions drawn from angular and local density corrected three-body distribution functions and the dihedral analysis.

3.2. Dynamics

3.2.1. Ligand exchange process

To investigate the mobility of ligands in the hydration shells, the mean residence times (MRT) were calculated using the direct method [64]. As discussed in previous sections, the first hydration shell around the thorium(IV) ion is flexible, but no water exchange processes with the second solvation shell were observed. Thus, the shell border radii were set to the following values: 1st shell:

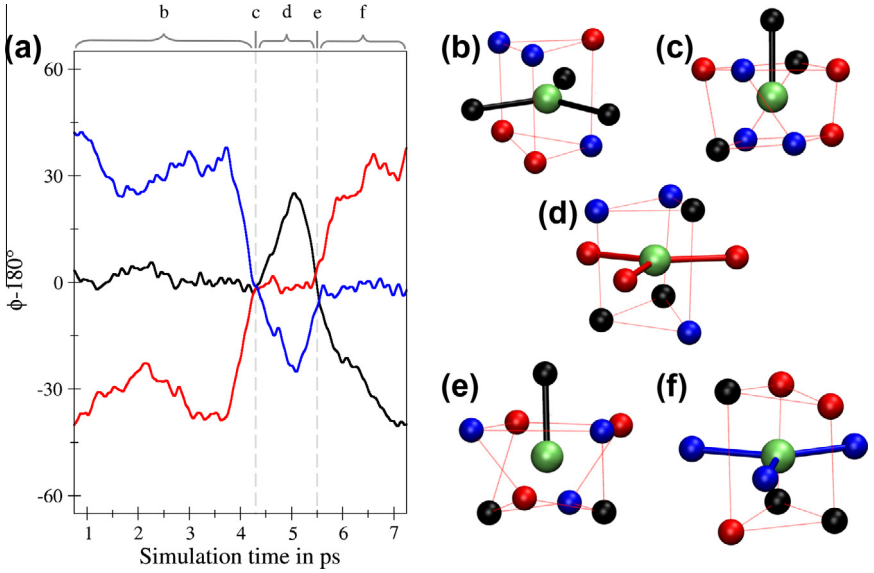

Fig. 5. (a) Selected O–Th–O–O dihedral angles as function of simulation time for a fraction of the simulation (black/red/blue: $O_{black/red/blue}$–Th–$O_{black/red/blue}$–$O_{black/red/blue}$). Angles are running averages, with a length of average of 0.5 ps, (b–f) snapshots demonstrating ligand re-orientations occurring during the simulation (green: thorium ion, others: oxygen atoms of the water molecules in the first coordination shell). Configurations (b, d, f) correspond to tricapped trigonal prism, (c and e) to monocapped square antiprism. (For interpretation of the references to color in this figure legend, the reader is referred to the web version of this article.)

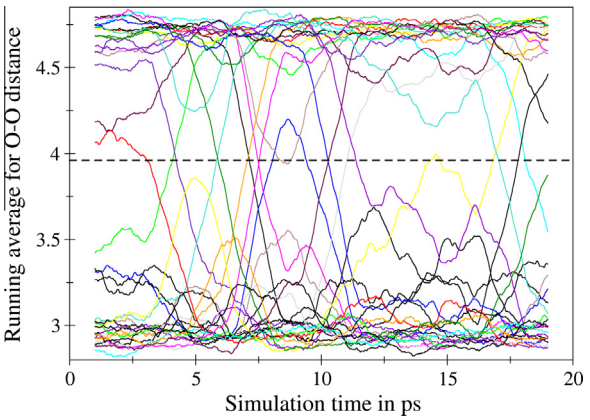

Fig. 6. Pair distances of all first-shell O–O pairs demonstrating the rapid dynamics occurring within the first hydration layer. Distances are running averages, with a length of average of 2 ps. The dashed line corresponds to the minimum of the local density corrected three body distribution function for the first shell as pointed out in Fig. 4a.

Table 1
Peak maxima of selected ion–O stretching frequencies (Q_{ion-O}) and corresponding force constants (k_{ion-O}).

Ion	Q_{ion-O} (cm^{-1})	k_{ion-O} (N m^{-1})	Ref.
Ce(IV)	420	149	[71]
Th(IV)	420	156	this work
U(IV)	–	157	[101]
Zr(IV)	484	188	[99]
Hf(IV)	–	212	[100]
Ir(III)	–	260	[104]

0.0–3.0 Å; 2nd shell: 3.2–5.7 Å; 3rd shell: 5.7–7.9 Å. Numerous water exchanges took place in the second and third hydration shell. Setting the t^*-value to 0.5 ps, 98 water exchanges between the second and third hydration shell were observed, yielding a mean residence time of 4.0 ps. For the third solvation layer 389 (t^* = 0.5 ps) water exchange events were found, which results in a MRT value of 2.0 ps. QM–MM MD studies on the structure and ultrafast dynamics of liquid water revealed a value of 1.6 ps (t^* = 0.5 ps, HF level of theory) for bulk water [81]. Thus it can be stated that the first, the second and even the third hydration layer of thorium(IV) are stabilized in comparison to pure water.

Additionally, the sustainability of the exchange processes S_{ex} was evaluated. This is done by comparing the number of all transitions (t^* = 0.0 ps) to the number of successful exchange events lasting at least 0.5 ps. Taking the inverse of the sustainability coefficient provides a measure of the average number of attempts required to achieve a successful exchange. For the second hydration layer, this number was calculated to be 3.5, and for the third solvation shell, a value of 5.4 was found. For bulk water the number of attempts per a lasting exchange event was determined to be 7.8 [81]. This series of sustainability coefficients again clearly shows the strong influence of the highly charged Th(IV) ion on the water ordering up to the third solvation shell.

Experimentally, water exchange studies on actinide aqua cations using ^{17}O NMR technique revealed a kinetic parameter of $k_{ex} > 5\times10^7\ s^{-1}$ (corresponding to a residence time of less than 20 ns) at room temperature for the $Th(H_2O)_{10}^{4+}$ species [102]. Numerous theoretical approaches are available aiming to clarify residence times of first- and second-shell water molecules of hydrated thorium: Yang et al. investigated water exchange mechanisms of the $Th(H_2O)_{10}^{4+}$ species via quantum chemical calculations and reported the lifetime of the intermediate $[Th(H_2O)_9]^{4+}\cdot H_2O$ to be 0.102 ns [96]. MD simulations by Réal et al. suggested a mean residence time of >10 ns for the water molecules of the first hydration shell, and 20.4 ± 4.7 ps for the second shell [103]. MD simulations with interaction potentials developed by B3LYP hybrid density functional calculations find a value of 423.4 ps for the residence time of a water molecule in the second hydration shell [91]. This value is rather high as B3LYP tends to predict water structure too rigid resulting in slower exchange rates (see discussion on choice of quantum theoretical level and basis set).

3.2.2. Vibrational analysis

Vibrational analysis using velocity autocorrelation functions and subsequent Fourier-transformation (FT) has been carried out to provide information on the ion-oxygen bond strength. The obtained wavenumbers offer a direct route for the determination of the binding force constants and can directly be compared to experimental Raman and/or IR spectra.

For the whole simulation of 20 ps, a value of 420 cm^{-1} was found, which corresponds to a force constant of 156 N/m. The strength of the ion–O bond is almost the same as for the U(IV) ion [101], but is still not as high as for the Zr(IV) [99] and Hf(IV) ions [100], which are themselves smaller than that of the enormously stable octahedrally coordinated hexaaqua-iridium(III) ion [104] (see Table 1). The wavenumber found is in excellent agreement with the experimental value of 420 cm^{-1} [105], which has been determined in very recent experiments on selective

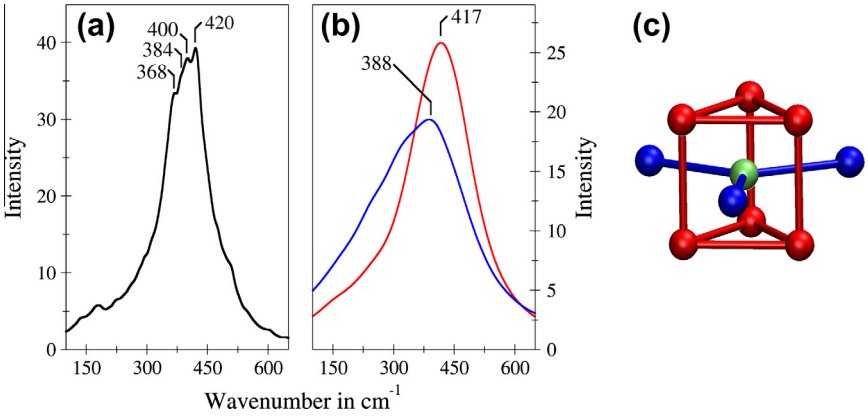

Fig. 7. Vibrational analysis using velocity autocorrelation functions followed by FT for (a) the whole 20 ps of simulation, for thorium(IV) with all oxygens within the first solvation layer, and (b) the first 4 ps of simulation, for the ion with the six prismatic (red) and the three capping (blue) water molecules separately. These two types of atoms are illustrated in c), the colors corresponding to those of plot (b). (For interpretation of the references to color in this figure legend, the reader is referred to the web version of this article.)

solid-phase extraction of thorium(IV) by Lin et al. [39], studies on the removal and recovery of thorium(IV) ions from aqueous solutions by Anirudhan et al. [106], and investigations on polynuclear thorium(IV) molecular clusters by Soderholm et al. [107,108].

In addition to the peak maximum at 420 cm^{-1}, side peaks at 400 and 368 cm^{-1}, and a small shoulder at 384 cm^{-1} were observed (see Fig. 7a). To investigate these peaks found using the whole simulation data, two additional calculations were carried out: (i) a velocity autocorrelation calculation followed by FT for the first 4 ps of simulation time only, and (ii) a vibrational analysis of a geometry-optimized $[Th(H_2O)_9]^{4+}$-cluster on Hartree–Fock level of theory, embedded in a polarizable continuum (GAUSSIAN 03). Investigation (i) was done, because there are no rearrangements in the first hydration shell during these 4 ps, and the hydration polyhedron was found to be tricapped trigonal prismatic. This provided the opportunity to clearly distinguish between the prismatic and the capping positions and to study these binding properties of each of the two species independently. This allowed the separate calculation of velocity autocorrelation functions for the ion–oxygen bond for the six prismatic water molecules on the one hand, and the three capping ones on the other hand. This analysis reveals two separate peaks at 417 and 388 cm^{-1} (153 and 133 N m^{-1}) (see Fig. 7b). At this point, it should be mentioned that the intensities are not significant after Fourier-transforming the VACF to a power spectrum. For (ii), the most intense peaks were found at 423 and 403, 390 and 377 cm^{-1}.

4. Conclusion

This work presents the first QMCF-MD-simulation of the tetravalent thorium ion in aqueous solution employing *ab initio* quantum mechanical means, thus intrinsically including many-body effects, charge transfer and polarization effects. The simulation does not only give valuable information on the hydration structure, but offers detailed insight into the ultrafast dynamical processes taking place within the hydration shells. Although the hydrate of this highly charged ion is stable in terms of hydrolysis in experiment and in this study, rapid solvent reorganizations within the first solvation shell make the hydrate a very flexible one. In order to study different aspects of this observed flexibility, a variety of methods of analysis were employed, including local density corrected three-body distribution functions and time series of dihedral angles and O–O distances. The simulation data provide evidence of a third hydration layer, showing properties clearly differing from bulk water. The performed vibrational analysis yielded results in excellent agreement with experimental data, however the simulation offered the possibility to investigate the binding of prismatic and capping oxygens independently.

Acknowledgments

Financial support from a PhD grant of the Leopold-Franzens-University of Innsbruck (Rector Univ. Prof. Dr. Dr.hc.mult. Tilmann D. Märk) for Lorenz R. Canaval is gratefully acknowledged.

References

[1] V. Dekoussar, G. Dyck, A. Galperin, C. Ganguly, M. Todosow, M. Yamawaki, Thorium fuel cycle – potential benefits and challenges, Tech. Rep., 2005.
[2] Z. Zhang, Z. Wu, D. Wang, Y. Xu, Y. Sun, F. Li, Y. Dong, Current status and technical description of Chinese 2 × 250 MW_{th} HTR-PM demonstration plant, Nucl. Eng. Des. 239 (7) (2009) 1212–1219.
[3] A.C. Kadak, A future for nuclear energy: pebble bed reactors, Int. J. Crit. Infrastruct. 1 (4) (2005) 330–345.
[4] P. Dent, Rare earth elements and permanent magnets, J. Appl. Phys. 111 (7) (2012) 07A721.
[5] M. Humphries, Rare Earth Elements: The Global Supply Chain, DIANE Publishing Company, 2010.
[6] L. Margonelli, Clean Energy's Dirty Little Secret. The Atlantic. Atlantic Media Company 05/2009. <http://www.theatlantic.com/magazine/archive/2009/05/clean-energys-dirty-little-secret/307377> (accessed 25.01.13.).
[7] S. Parry, E. Douglas, In China, The True Cost of Britain's Clean, Green Wind Power Experiment: Pollution on a Disastrous Scale. Daily Mail. Associated Newspapers Ltd. 26.01.2011. <http://www.dailymail.co.uk/home/moslive/article-1350811/In-China-true-cost-Britains-clean-green-wind-power-experiment-Pollution-disastrous-scale.html> (accessed 25.01.13).
[8] H. von Buttlar, Das schmutzige Geheimnis der Energiewende, Financial Times Deutschland, G + J Wirtschaftsmedien GmbH & Co. KG 15.08.2012. <http://www.ftd.de/politik/deutschland/:windkraft-das-schmutzige-geheimnis-der-energiewende/70076643.html> (accessed 25.01.13).
[9] T.P. Rao, P. Metilda, J.M. Gladis, Preconcentration techniques for uranium(IV) and thorium(IV) prior to analytical determination – an overview, Talanta 68 (4) (2006) 1047–1064.
[10] M. Schmidt, S. Lee, R. Wilson, L. Soderholm, P. Fenter, Sorption of tetravalent thorium on muscovite, Geochim. Cosmochim. Acta 88 (2012) 66–76.
[11] L. Yan, F. Qiaohui, W. Wangsuo, Sorption of Th(IV) on goethite: effects of pH, ionic strength, FA and phosphate, J. Radioanal. Nucl. Chem. 289 (2011) 865–871.
[12] D. Pan, Q. Fan, K. Ding, P. Li, Y. Lu, T. Yu, J. Xu, W. Wu, The sorption mechanisms of Th(IV) on attapulgite, Sci. China Chem. 54 (2011) 1138–1147.
[13] L. Chen, X. Gao, Thermodynamic study of Th(IV) sorption on attapulgite, Appl. Radiat. Isotopes 67 (1) (2009) 1–6.
[14] Y. Khazaei, H. Faghihian, M. Kamali, Removal of thorium from aqueous solutions by sodium clinoptilolite, J. Radioanal. Nucl. Chem. 289 (2011) 529–536.
[15] D. Pan, Q. Fan, P. Li, S. Liu, W. Wu, Sorption of Th(IV) on Na-bentonite: effects of pH, ionic strength, humic substances and temperature, Chem. Eng. J. 172 (2–3) (2011) 898–905.
[16] T.S. Anirudhan, S. Rijith, A.R. Tharun, Adsorptive removal of thorium(IV) from aqueous solutions using poly(methacrylic acid)-grafted chitosan/bentonite composite matrix: process design and equilibrium studies, Colloid. Surface. A 368 (1–3) (2010) 13–22.
[17] S.R. Yousefi, S.J. Ahmadi, F. Shemirani, M.R. Jamali, M. Salavati-Niasari, Simultaneous extraction and preconcentration of uranium and thorium in aqueous samples by new modified mesoporous silica prior to inductively coupled plasma optical emission spectrometry determination, Talanta 80 (1) (2009) 212–217.
[18] P. Sharma, G. Singh, R. Tomar, Synthesis and characterization of an analogue of heulandite: sorption applications for thorium(IV), europium(III), samarium(II) and iron(III) recovery from aqueous waste, J. Colloid Interface Sci. 332 (2) (2009) 298–308.
[19] I. Rojo, F. Seco, M. Rovira, J. Giménez, G. Cervantes, V. Martí, J. de Pablo, Thorium sorption onto magnetite and ferrihydrite in acidic conditions, J. Nucl. Mater. 385 (2) (2009) 474–478.
[20] Z. Talip, M. Eral, U. Hiçsönmez, Adsorption of thorium from aqueous solutions by perlite, J. Environ. Radioact. 100 (2) (2009) 139–143.
[21] G. Sheng, J. Hu, X. Wang, Sorption properties of Th(IV) on the raw diatomite – effects of contact time, pH, ionic strength and temperature, Appl. Radiat. Isotopes 66 (10) (2008) 1313–1320.
[22] D.L. Guerra, R.R. Viana, C. Airoldi, Adsorption of thorium(IV) on chemically modified amazon clays, J. Braz. Chem. Soc. 20 (2009) 1164–1174.
[23] D. Zhao, S. Feng, C. Chen, S. Chen, D. Xu, X. Wang, Adsorption of thorium(IV) on MX-80 bentonite: effect of pH, ionic strength and temperature, Appl. Clay Sci. 41 (1–2) (2008) 17–23.
[24] D. Xu, C. Chen, X. Tan, J. Hu, X. Wang, Sorption of Th(IV) on Na-rectorite: effect of HA, ionic strength, foreign ions and temperature, Appl. Geochem. 22 (12) (2007) 2892–2906.
[25] C. Chen, X. Wang, Influence of pH, soil humic/fulvic acid, ionic strength and foreign ions on sorption of thorium(IV) onto γ-Al_2O_3, Appl. Geochem. 22 (2) (2007) 436–445.
[26] X. Tan, X. Wang, C. Chen, A. Sun, Effect of soil humic and fulvic acids, pH and ionic strength on Th(IV) sorption to TiO_2 nanoparticles, Appl. Radiat. Isotopes 65 (4) (2007) 375–381.
[27] X. Tan, X. Wang, M. Fang, C. Chen, Sorption and desorption of Th(IV) on nanoparticles of anatase studied by batch and spectroscopy methods, Colloid. Surface. A 296 (1–3) (2007) 109–116.
[28] C. Chen, X. Wang, Sorption of Th(IV) to silica as a function of pH, humic/fulvic acid, ionic strength, electrolyte type, Appl. Radiat. Isotopes 65 (2) (2007) 155–163.
[29] D. Humelnicu, G. Drochioiu, M. Sturza, A. Cecal, K. Popa, Kinetic and thermodynamic aspects of U(VI) and Th(IV) sorption on a zeolitic volcanic tuff, J. Radioanal. Nucl. Chem. 270 (3) (2006) 637–640.
[30] Z. Hongxia, D. Zheng, T. Zuyi, Sorption of thorium(IV) ions on gibbsite: effects of contact time, pH, ionic strength, concentration, phosphate and fulvic acid, Colloid. Surface. A 278 (1–3) (2006) 46–52.
[31] T.S. Anirudhan, S. Rijith, V.R.N. Ratheesh, A highly efficient carboxyl-terminated hybrid adsorbent composite matrix for the adsorption of uranium(VI) and thorium(IV) from aqueous solutions and nuclear industry effluents, Desalin. Water Treat. 38 (1–3) (2012) 79–89.
[32] V. Dedkova, O. Shvoeva, S. Savvin, Complexation of zirconium(IV), thorium(IV) and uranium(VI) malonates with Arsenazo III and Arsenazo M on fiber ion exchangers, J. Anal. Chem. 67 (2012) 527–530.

[33] M. Hosseini, A. Hosseini-Bandegharaei, Selective extraction of Th(IV) over U(VI) and other co-existing ions using eosin B-impregnated Amberlite IRA-410 resin beads, J. Radioanal. Nucl. Chem. 283 (1) (2010) 23–30.

[34] T.S. Anirudhan, S.R. Rejeena, Thorium(IV) removal and recovery from aqueous solutions using tannin-modified poly(glycidylmethacrylate)-grafted zirconium oxide densified cellulose, Ind. Eng. Chem. Res. 50 (23) (2011) 13288–13298.

[35] A. Hosseini-Bandegharaei, M.S. Hosseini, Y. Jalalabadi, M. Nedaie, M. Sarwghadi, A. Taherian, E. Hosseini, A novel extractant-impregnated resin containing carminic acid for selective separation and pre-concentration of uranium(VI) and thorium(IV), Int. J. Environ. Anal. Chem. 93 (1) (2011) 108–124.

[36] L. Zuo, S. Yu, H. Zhou, X. Tian, J. Jiang, Th(IV) adsorption on mesoporous molecular sieves: effects of contact time, solid content, pH, ionic strength, foreign ions and temperature, J. Radioanal. Nucl. Chem. 288 (2) (2011) 379–387.

[37] M. Clark, J. Harrison, T. Payne, The pH-dependence and reversibility of uranium and thorium binding on a modified bauxite refinery residue using isotopic exchange techniques, J. Colloid Interface Sci. 356 (2) (2011) 699–705.

[38] F.A. Aydin, M. Soylak, Separation, preconcentration and inductively coupled plasma-mass spectrometric (ICP-MS) determination of thorium(IV), titanium(IV), iron(III), lead(II) and chromium(III) on 2-nitroso-1-naphthol impregnated MCI GEL CHP20P resin, J. Hazard. Mater. 173 (1–3) (2010) 669–674.

[39] C. Lin, H. Wang, Y. Wang, Z. Cheng, Selective solid-phase extraction of trace thorium(IV) using surface-grafted Th(IV)-imprinted polymers with pyrazole derivative, Talanta 81 (1–2) (2010) 30–36.

[40] S. Sabale, D. Jadhav, B. Mohite, Sorption study of U(VI), Th(IV) and Ce(III) on poly [dibenzo-18-crown-6] in L-arginine to develop sequential column chromatographic separation method, J. Radioanal. Nucl. Chem. 284 (2) (2010) 273–278.

[41] S. Seyhan, M. Merdivan, N. Demirel, Use of o-phenylene dioxydiacetic acid impregnated in Amberlite XAD resin for separation and preconcentration of uranium(VI) and thorium(IV), J. Hazard. Mater. 152 (1) (2008) 79–84.

[42] S. Ansari, P. Mohapatra, V. Manchanda, Synthesis of N, N′-dimethyl-N, N′-dibutyl malonamide functionalized polymer and its sorption affinities towards U(VI) and Th(IV) ions, Talanta 73 (5) (2007) 878–885.

[43] E. Bursali, M. Merdivan, M. Yurdakoc, Preconcentration of uranium(VI) and thorium(IV) from aqueous solutions using low-cost abundantly available sorbent, J. Radioanal. Nucl. Chem. 283 (2010) 471–476.

[44] C. Kütahyalı, M. Eral, Sorption studies of uranium and thorium on activated carbon prepared from olive stones: kinetic and thermodynamic aspects, J. Nucl. Mater. 396 (2–3) (2010) 251–256.

[45] A. Khan, L. Paquiza, A. Khan, An advanced nano-composite cation-exchanger polypyrrole zirconium titanium phosphate as a Th(IV)-selective potentiometric sensor: preparation, characterization and its analytical application, J. Mater. Sci. 45 (13) (2010) 3610–3625.

[46] S. Hassan, E. Elnemma, A. Attawiya, Novel thorium membrane sensors with anionic response based on trioctylphosphine oxide and toluate ionophores, Electroanalysis 20 (19) (2008) 2063–2069.

[47] A. Joshi, N. Sebastian, K. Kate, D. Ghadse, Coated wire thorium ion selective electrode: Part I, J. Radioanal. Nucl. Chem. 286 (1) (2010) 115–119.

[48] A. Joshi, N. Sebastian, K. Kate, D. Ghadse, Coated wire thorium ion selective electrode: Part II, J. Radioanal. Nucl. Chem. 288 (2) (2011) 595–597.

[49] R. Spezia, C. Beuchat, R. Vuilleumier, P. DAngelo, L. Gagliardi, Unravelling the hydration structure of ThX_4 (X = Br, Cl) water solutions by molecular dynamics simulations and X-ray absorption spectroscopy, J. Phys. Chem. B 116 (22) (2012) 6465–6475.

[50] T. Hofer, A. Pribil, B. Randolf, B. Rode, Ab initio quantum mechanical charge field molecular dynamics: a nonparametrized first-principle approach to liquids and solutions, Adv. Quantum Chem. 59 (2010) 213–246.

[51] A.K.H. Weiss, T.S. Hofer, Exploiting the capabilities of quantum chemical simulations to characterise the hydration of molecular compounds, RSC Adv. 3 (2013) 1606–1635.

[52] M.J. Field, P.A. Bash, M. Karplus, A combined quantum mechanical and molecular mechanical potential for molecular dynamics simulations, J. Comput. Chem. 11 (6) (1990) 700–733.

[53] D. Bakowies, W. Thiel, Hybrid models for combined quantum mechanical and molecular mechanical approaches, J. Phys. Chem. 100 (25) (1996) 10580–10594.

[54] J. Gao, Potential of mean force for the isomerization of DMF in aqueous solution: a Monte Carlo QM/MM simulation study, J. Am. Chem. Soc. 115 (7) (1993) 2930–2935.

[55] F.H. Stillinger, A. Rahman, Revised central force potentials for water, J. Chem. Phys. 68 (2) (1978) 666–670.

[56] P. Bopp, G. Jancs, K. Heinzinger, An improved potential for non-rigid water molecules in the liquid phase, Chem. Phys. Lett. 98 (2) (1983) 129–133.

[57] R.S. Mulliken, Electronic population analysis on LCAO[single bond]MO molecular wave functions. I, J. Chem. Phys. 23 (10) (1955) 1833–1840.

[58] R.S. Mulliken, Electronic population analysis on LCAO[single bond]MO molecular wave functions. II. Overlap populations, bond orders, and covalent bond energies, J. Chem. Phys. 23 (10) (1955) 1841–1846.

[59] T.S. Hofer, A.K. Weiss, B.R. Randolf, B.M. Rode, Hydration of highly charged ions, Chem. Phys. Lett. 512 (4–6) (2011) 139–145.

[60] A.K.H. Weiss, T.S. Hofer, B.R. Randolf, B.M. Rode, Guanidinium in aqueous solution studied by quantum mechanical charge field-molecular dynamics (QMCF-MD), Phys. Chem. Chem. Phys. 14 (2012) 7012–7027.

[61] A. Weiss, T. Hofer, B. Randolf, A. Bhattacharjee, B. Rode, Hydrogen bond formation of formamide and N-methylformamide in aqueous solution studied by quantum mechanical charge field-molecular dynamics (QMCF-MD), Phys. Chem. Chem. Phys. 13 (2011) 12173–12185.

[62] B. Rode, T. Hofer, M. Kugler, The Basics of Theoretical and Computational Chemistry, Wiley-VCH, 2007.

[63] A. Bhattacharjee, T.S. Hofer, B.M. Rode, Local density corrected three-body distribution functions for probing local structure reorganization in liquids, Phys. Chem. Chem. Phys. 10 (2008) 6653–6657.

[64] T.S. Hofer, H.T. Tran, C.F. Schwenk, B.M. Rode, Characterization of dynamics and reactivities of solvated ions by ab initio simulations, J. Comput. Chem. 25 (2) (2004) 211–217.

[65] P. Bopp, A study of the vibrational motions of water in an aqueous $CaCl_2$ solution, Chem. Phys. 106 (2) (1986) 205–212.

[66] E. Spohr, G. Palinkas, K. Heinzinger, P. Bopp, M.M. Probst, Molecular dynamics study of an aqueous strontium chloride solution, J. Phys. Chem. 92 (23) (1988) 6754–6761.

[67] A.P. Scott, L. Radom, Harmonic vibrational frequencies: an evaluation of Hartree–Fock, Møller–Plesset, quadratic configuration interaction, density functional theory, and semiempirical scale factors, J. Phys. Chem. 100 (41) (1996) 16502–16513.

[68] D. DeFrees, A. McLean, Molecular orbital predictions of the vibrational frequencies of some molecular ions, J. Chem. Phys. 82 (1985) 333.

[69] H.J.C. Berendsen, J.P.M. Postma, W.F. van Gunsteren, A. DiNola, J.R. Haak, Molecular dynamics with coupling to an external bath, J. Chem. Phys. 81 (8) (1984) 3684–3690.

[70] D.J. Adams, E.M. Adams, G.J. Hills, The computer simulation of polar liquids, Mol. Phys. 38 (2) (1979) 387–400.

[71] O.M.D. Lutz, T.S. Hofer, B.R. Randolf, A.K.H. Weiss, B.M. Rode, A QMCF-MD investigation of the structure and dynamics of Ce^{4+} in aqueous solution, Inorg. Chem. 51 (12) (2012) 6746–6752.

[72] TURBOMOLE V6.3 2011, A Development of University of Karlsruhe and Forschungszentrum Karlsruhe GmbH, 1989–2007, TURBOMOLE GmbH, since 2007. <http://www.turbomole.com>.

[73] R. Ahlrichs, M. Bar, M. Häser, H. Horn, C. Kolmel, Electronic structure calculations on workstation computers: the program system turbomole, Chem. Phys. Lett. 162 (3) (1989) 165–169.

[74] M. Häser, R. Ahlrichs, Improvements on the direct SCF method, J. Comput. Chem. 10 (1) (1989) 104–111.

[75] J. Dunning, H. Thomas, Gaussian basis functions for use in molecular calculations. I. Contraction of (9s5p) atomic basis sets for the first-row atoms, J. Chem. Phys. 53 (7) (1970) 2823–2833.

[76] K.L. Schuchardt, B.T. Didier, T. Elsethagen, L. Sun, V. Gurumoorthi, J. Chase, J. Li, T.L. Windus, Basis set exchange: a community database for computational sciences, J. Chem. Inf. Model. 47 (3) (2007) 1045–1052.

[77] D. Feller, The role of databases in support of computational chemistry calculations, J. Comput. Chem. 17 (13) (1996) 1571–1586.

[78] W.C. Ermler, R.B. Ross, P.A. Christiansen, Ab initio relativistic effective potentials with spin-orbit operators. VI. Fr through Pu, Int. J. Quantum Chem. 40 (6) (1991) 829–846.

[79] W. Küchle, M. Dolg, H. Stoll, H. Preuss, Energy-adjusted pseudopotentials for the actinides. parameter sets and test calculations for thorium and thorium monoxide, J. Chem. Phys. 100 (10) (1994) 7535–7542.

[80] M.J. Frisch, G.W. Trucks, H.B. Schlegel, G.E. Scuseria, M.A. Robb, J.R. Cheeseman, J.A. Montgomery Jr., T. Vreven, K.N. Kudin, J.C. Burant, J.M. Millam, S.S. Iyengar, J. Tomasi, V. Barone, B. Mennucci, M. Cossi, G. Scalmani, N. Rega, G.A. Petersson, H. Nakatsuji, M. Hada, M. Ehara, K. Toyota, R. Fukuda, J. Hasegawa, M. Ishida, T. Nakajima, Y. Honda, O. Kitao, H. Nakai, M. Klene, X. Li, J.E. Knox, H.P. Hratchian, J.B. Cross, V. Bakken, C. Adamo, J. Jaramillo, R. Gomperts, R.E. Stratmann, O. Yazyev, A.J. Austin, R. Cammi, C. Pomelli, J.W. Ochterski, P.Y. Ayala, K. Morokuma, G.A. Voth, P. Salvador, J.J. Dannenberg, V.G. Zakrzewski, S. Dapprich, A.D. Daniels, M.C. Strain, O. Farkas, D.K. Malick, A.D. Rabuck, K. Raghavachari, J.B. Foresman, J.V. Ortiz, Q. Cui, A.G. Baboul, S. Clifford, J. Cioslowski, B.B. Stefanov, G. Liu, A. Liashenko, P. Piskorz, I. Komaromi, R.L. Martin, D.J. Fox, T. Keith, M.A. Al-Laham, C.Y. Peng, A. Nanayakkara, M. Challacombe, P.M.W. Gill, B. Johnson, W. Chen, M.W. Wong, C. Gonzalez, J.A. Pople, Gaussian 03, Revision C.02, Gaussian, Inc., Wallingford, CT, 2004.

[81] D. Xenides, B.R. Randolf, B.M. Rode, Structure and ultrafast dynamics of liquid water: a quantum mechanics/molecular mechanics molecular dynamics simulations study, J. Chem. Phys. 122 (17) (2005) 174506.

[82] J. Schmidt, J. VandeVondele, I.-F.W. Kuo, D. Sebastiani, J.I. Siepmann, J. Hutter, C.J. Mundy, Isobaric–isothermal molecular dynamics simulations utilizing density functional theory: an assessment of the structure and density of water at near-ambient conditions, J. Phys. Chem. B 113 (35) (2009) 11959–11964.

[83] S. Yoo, X.C. Zeng, S.S. Xantheas, On the phase diagram of water with density functional theory potentials: the melting temperature of ice I_h with the Perdew–Burke–Ernzerhof and Becke–Lee–Yang–Parr functionals, J. Chem. Phys. 130 (2009) 221102.

[84] D.A. Pantazis, F. Neese, All-electron scalar relativistic basis sets for the actinides, J. Chem. Theory Comput. 7 (3) (2011) 677–684.

[85] H. Moll, M.A. Denecke, F. Jalilehvand, M. Sandström, I. Grenthe, Structure of the aqua ions and fluoride complexes of uranium(IV) and thorium(IV) in aqueous solution an EXAFS study, Inorg. Chem. 38 (8) (1999) 1795–1799.
[86] M. Sandström, I. Persson, F. Jalilehvand, P. Lindquist-Reis, D. Spångberg, K. Hermansson, Hydration of some large and highly charged metal ions, J. Synchrotron Radiat. 8 (2) (2001) 657–659.
[87] C. Hennig, K. Schmeide, V. Brendler, H. Moll, S. Tsushima, A.C. Scheinost, EXAFS Investigation of U(VI), U(IV), and Th(IV) sulfato complexes in aqueous solution, Inorg. Chem. 46 (15) (2007) 5882–5892.
[88] J. Rothe, M.A. Denecke, V. Neck, R. Müller, J.I. Kim, XAFS investigation of the structure of aqueous thorium(IV) species, colloids, and solid thorium(IV) oxide/hydroxide, Inorg. Chem. 41 (2) (2002) 249–258.
[89] G. Johansson, M. Magini, H. Ohtaki, Coordination around thorium(IV) in aqueous perchlorate, chloride and nitrate solutions, J. Solution Chem. 20 (1991) 775–792.
[90] R. Wilson, S. Skanthakumar, P. Burns, L. Soderholm, Structure of the homoleptic thorium(IV) aqua ion $[Th(H_2O)_{10}]Br_4$, Angew. Chem. 119 (42) (2007) 8189–8191.
[91] T. Yang, S. Tsushima, A. Suzuki, Quantum mechanical and molecular dynamical simulations on thorium(IV) hydrates in aqueous solution, J. Phys. Chem. A 105 (45) (2001) 10439–10445.
[92] F. Réal, M. Trumm, V. Vallet, B. Schimmelpfennig, M. Masella, J.-P. Flament, Quantum chemical and molecular dynamics study of the coordination of Th(IV) in aqueous solvent, J. Phys. Chem. B 114 (48) (2010) 15913–15924.
[93] A. Fratiello, R.E. Lee, R.E. Schuster, Proton magnetic resonance hydration study of scandium, yttrium, and thorium perchlorate in water-acetone mixtures, Inorg. Chem. 9 (2) (1970) 391–392.
[94] T. Yang, S. Tsushima, A. Suzuki, Chloride concentration and temperature effects on the hydration of Th(IV) ion: a molecular dynamics simulation, Chem. Phys. Lett. 360 (5–6) (2002) 534–542.
[95] S. Tsushima, T. Yang, Y. Mochizuki, Y. Okamoto, Ab initio study on the structures of Th(IV) hydrate and its hydrolysis products in aqueous solution, Chem. Phys. Lett. 375 (1–2) (2003) 204–212.
[96] T. Yang, S. Tsushima, A. Suzuki, The water exchange mechanism in thorium(IV) hydrates as studied by quantum chemical methods, J. Solid State Chem. 171 (1–2) (2003) 235–241.
[97] E.N. Rizkalla, G.R. Choppin, in: L.E.G.R.C. Karl, A. Gschneidner Jr., G.H. Lander (Eds.), Lanthanides/Actinides: Chemistry, Handbook on the Physics and Chemistry of Rare Earths, Vol. 18, Elsevier, 1994, pp. 529–558.
[98] T.S. Hofer, B.R. Randolf, B.M. Rode, Al(III) hydration revisited: an ab initio quantum mechanical charge field molecular dynamics study, J. Phys. Chem. B 112 (37) (2008) 11726–11733.
[99] C.B. Messner, T.S. Hofer, B.R. Randolf, B.M. Rode, Structure and dynamics of the Zr4+ ion in water, Phys. Chem. Chem. Phys. 13 (2011) 224–229.
[100] C.B. Messner, T.S. Hofer, B.R. Randolf, B.M. Rode, Computational study of the hafnium(IV) ion in aqueous solution, Chem. Phys. Lett. 501 (4–6) (2011) 292–295.
[101] R.J. Frick, A.B. Pribil, T.S. Hofer, B.R. Randolf, A. Bhattacharjee, B.M. Rode, Structure and dynamics of the U4+ ion in aqueous solution: an ab initio quantum mechanical charge field molecular dynamics study, Inorg. Chem. 48 (9) (2009) 3993–4002.
[102] I. Farkas, I. Grenthe, I. Bányai, The rates and mechanisms of water exchange of actinide aqua ions: a variable temperature ^{17}O NMR study of $U(H_2O)_{10}^{4+}$, $UF(H_2O)_9^{3+}$, and $Th(H_2O)_{10}^{4+}$, J. Phys. Chem. A 104 (6) (2000) 1201–1206.
[103] F. Réal, M. Trumm, B. Schimmelpfennig, M. Masella, V. Vallet, Further insights in the ability of classical nonadditive potentials to model actinide ion–water interactions, J. Comput. Chem. 34 (9) (2013) 707–719.
[104] P. Pedevilla, T. Hofer, B. Randolf, B. Rode, Simulation of Ir(III) in aqueous solution: the most inert ion hydrate, Aust. J. Chem. 65 (2012) 1582–1586.
[105] K. Nakamoto, Infrared and Raman Spectra of Inorganic and Coordination Compounds, fourth ed., John Wiley & Sons, New York, 1986.
[106] T.S. Anirudhan, P.S. Suchithra, P. Senan, A.R. Tharun, Kinetic and equilibrium profiles of adsorptive recovery of thorium(IV) from aqueous solutions using poly(methacrylic acid) grafted cellulose/bentonite superabsorbent composite, Ind. Eng. Chem. Res. 51 (13) (2012) 4825–4836.
[107] M. Vasiliu, K.E. Knope, L. Soderholm, D.A. Dixon, Spectroscopic and energetic properties of thorium(IV) molecular clusters with a hexanuclear core, J. Phys. Chem. A 116 (25) (2012) 6917–6926.
[108] K.E. Knope, M. Vasiliu, D.A. Dixon, L. Soderholm, Thorium(IV)–selenate clusters containing an octanuclear Th(IV) hydroxide/oxide core, Inorg. Chem. 51 (7) (2012) 4239–4249.